Stable Isotopic Characterization of Nitrate Wet Deposition in the Tropical Urban Atmosphere of Costa Rica

Mario Villalobos-Forbes
Universidad Nacional de Costa Rica

Germain Esquivel-Hernandez (✉ germain.esquivel.hernandez@una.cr)
Universidad Nacional de Costa Rica   https://orcid.org/0000-0002-6890-6509

Ricardo Sánchez-Murillo
Universidad Nacional de Costa Rica

Rolando Sánchez-Gutiérrez
Universidad Nacional de Costa Rica

Ioannis Matiatos
International Energy Agency

Stable isotopic characterization of nitrate wet deposition in the tropical urban atmosphere of Costa Rica

Mario Villalobos-Forbes[1,2,] Germain Esquivel-Hernández[1,2*], Ricardo Sánchez-Murillo[1,2], Rolando Sánchez-Gutiérrez[1,2], Ioannis Matiatos[3]

[1]Stable Isotopes Research Group, Chemistry Department, Universidad Nacional Costa Rica, Heredia 86-3000, Costa Rica

[2]Water Resources Management Laboratory, Chemistry Department, Universidad Nacional Costa Rica, Heredia 86-3000, Costa Rica

[3]International Atomic Energy Agency, Isotope Hydrology Section, Vienna International Centre, 1400 Vienna, Austria

* Correspondence: germain.esquivel.hernandez@una.cr; Tel.: +506 2277-3484; Fax: +506 2277-3349

Abstract

Increasing energy consumption and food production worldwide results in anthropogenic emissions of reactive nitrogen into the atmosphere. To date, however, little information is available on tropical urban environments where inorganic nitrogen is vastly transported and deposited through precipitation on terrestrial and aquatic ecosystems. To fill this gap, we present compositions of water stable isotopes in precipitation and atmospheric nitrate ($\delta^{18}O$-H_2O, δ^2H-H_2O, $\delta^{15}N$-NO_3^-, and $\delta^{18}O$-NO_3^-) collected daily between August 2018 and November 2019 in a tropical urban atmosphere of central Costa Rica. Rainfall generation processes (convective and stratiform) were identified using stable isotopes in precipitation combined with air mass back trajectory analysis. A Bayesian isotope mixing model forced with $\delta^{15}N$-NO_3^- values corrected for potential ^{15}N fractionation effects reveal the predominant contribution of biomass burning and lightning to nitrate wet deposition. $\delta^{18}O$-NO_3^- values in Caribbean convective rainfall reflect the oxidation chemistry of NO_x sources whereas $\delta^{15}N$-NO_3^- values in Pacific stratiform rainfall indicate the transport of nitrogen sources contributing to nitrate in atmospheric deposition. These findings provide necessary baseline information about the combination of water and nitrogen stable isotopes with atmospheric chemistry and hydrometeorological techniques to better understand wet deposition processes and to characterize the origin of inorganic nitrogen loadings in tropical regions.
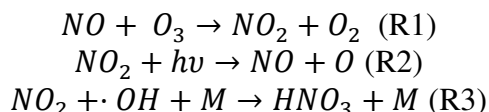
Keywords: stable isotopes; nitrate; wet deposition; rainfall generation processes; urban atmosphere; Costa Rica
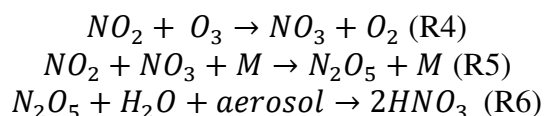
1. Introduction

Since the beginning of the industrialization era, human activities have dramatically increased the amounts of reactive nitrogen emitted to the atmosphere and deposited to the terrestrial and aquatic ecosystems, modifying the biogeochemical cycle of nitrogen (Harrison 2018; Kanakidou et al. 2016; Michalski et al. 2011). Anthropogenic emissions of reactive nitrogen come mainly from fossil fuels combustion (~30 Tg N/yr), accounting for

more than 50% of the total global emissions. Agriculture emissions (e.g., from fertilized soils) were estimated in 8 Tg N/yr. Other reactive nitrogen emissions include biomass burning (~5 Tg N/yr), biogenic soil processes (~18 Tg N/yr) and lighting (up to 5 Tg N/yr) (Fowler et al. 2013). Emissions of nitrogen oxides ($NO_x = NO + NO_2$) are of interest as they are important drivers of atmospheric chemistry since tropospheric ozone production is controlled by their availability (Fang et al. 2011; Wallington et al. 2019). Nitric acid (HNO_3) or nitrate (NO_3^-) are the major sink of NO_x and major contributors to the atmospheric acidity, placing second after sulfuric acid (H_2SO_4). Ammonia (NH_3) also plays an important role as it is the main neutralizing gas for these acidic compounds (Beyn et al. 2015; Felix et al. 2017; Kanakidou et al. 2016). Therefore, identifying the mechanisms controlling the transformation of NO_x into nitrate and its deposition (e.g., through precipitation) is important to underpin the potential impacts on the nitrogen cycles from local to regional and global scales.

The combination of environmental stable isotopes with atmospheric chemistry and hydrometeorological techniques is promising for gathering crucial information about the sources and cycling of nitrogen species beyond what concentration measurements alone can provide (Elliot et al. 2019; Hastings and Sigman 2003; Xiao et al. 2015). Overall, the oxidation mechanism of nitrogen in polluted atmospheres is controlled by O_3 and $\cdot OH$ during the day via:

$$NO + O_3 \rightarrow NO_2 + O_2 \text{ (R1)}$$
$$NO_2 + hv \rightarrow NO + O \text{ (R2)}$$
$$NO_2 + \cdot OH + M \rightarrow HNO_3 + M \text{ (R3)}$$

and at night via:

$$NO_2 + O_3 \rightarrow NO_3 + O_2 \text{ (R4)}$$
$$NO_2 + NO_3 + M \rightarrow N_2O_5 + M \text{ (R5)}$$
$$N_2O_5 + H_2O + aerosol \rightarrow 2HNO_3 \text{ (R6)}$$

In reaction 5, M is commonly N_2 or O_2 and stabilizes the product through collisions. Based on these reactions, it is possible to quantify the equilibrium fractionation of nitrogen isotopes associated with NO_x oxidation and HNO_3 formation pathways using mixing models that rely on the assumptions of two major NO_x oxidation and HNO_3 formation pathways (i.e., OH: daytime (R1-3) and N_2O_5: nighttime (R4-6)) (Song et al., 2019; Felix and Murgulet, 2020). Oxygen and nitrogen stable isotope ratios of nitrate can also be used to collect additional information about the sources and sinks of atmospheric nitrate. Nitrogen stable isotope ratios in atmospheric nitrate ($\delta^{15}N\text{-}NO_3^-$) can be used to trace NO_x sources. Source identification is possible due to the different $\delta^{15}N\text{-}NO_3^-$ signature of the potential endmembers, but the ^{15}N isotopic fractionation during the conversion of NO_x to nitrate needs to be considered (Liu et al. 2017; Michalski et al. 2011, Felix and Murgulet, 2020). On this matter, $\delta^{18}O\text{-}NO_3^-$ can provide information on the nature and the relative importance of NO_x oxidation pathways, ultimately leading to atmospheric nitrate (Fang et al. 2011; Savarino et al. 2013). However, the interpretation of this isotope information is more complicated and limited because $\delta^{18}O\text{-}NO_3^-$ is related to the mixing of different

92 oxygen sources (e.g., O_3, H_2O, $\cdot OH$) and isotopic fractionation during the photochemical
93 conversion of NO_x into NO_3^- (Michalski et al. 2011; Xiao et al. 2015).
94   In tropical regions like Central America, the formation of deep convective systems
95 is an important component of regional precipitation intensity and distribution (Durán-
96 Quesada et al. 2017). The deep convective activity is related to the influence of Mesoscale
97 Convective Systems (MCSs) and the formation of convective rainfall (i.e., small-scale
98 systems: 1-2 km and high intensity precipitation) and stratiform rainfall (i.e., large scale
99 ~100 km and low intensity precipitation) (Sánchez-Murillo et al. 2015, 2016). For the high-
100 intensity convective and lower-intensity stratiform systems, differences in vertical air
101 motions and microphysical processes govern the rain formation. Thus, these rainfall
102 generation processes impart characteristic water isotopic compositions (δ^2H and $\delta^{18}O$) to
103 convective and stratiform precipitation due to the condensation and riming associated with
104 boundary layer moisture (Aggarwal et al. 2016; Konecky et al., 2019). For instance,
105 stratiform rainfall related with MCSs has been shown to be mainly associated with large
106 negative excursions of $\delta^{18}O$ and δ^2H values in tropical rainfall (Kurita 2013; Sánchez-
107 Murillo et al. 2019). For two sites in Costa Rica, the average stratiform rainfall fraction
108 contributing to each precipitation event was modeled using a statistically significant
109 relationships of stratiform rainfall area fractions and the isotopic composition of
110 precipitation (i.e., $\delta^{18}O$; Munksgaard et al. 2019).

111   Regarding the ion composition of precipitation, rainfall from stratiform clouds
112 showed higher ion concentrations and lower pH than convective rainfall in tropical forests
113 of Congo and Amazonia (Andreae et al. 1990; Lacaux et al. 1992). This finding seems to be
114 linked to the higher liquid water content in convective clouds, which leads to a dilution of
115 the chemical content of the precipitation (Lacaux et al. 1992). However, little information is
116 available for regions like Central America where rainfall is defined by the intersection of
117 large-scale circulation patterns, the moisture inputs from the Caribbean Sea and the Pacific
118 Ocean, and local processes in which topography and vegetation cover play a relevant role
119 (Sánchez-Murillo et al., 2020). Recent observations in the mixing ratios of trace gases (e.g.,
120 carbon dioxide and methane) in the urban area of Costa Rica indicate that there is a strong
121 influence of the local atmospheric mixing conditions on the dispersion and chemical
122 transformations of atmospheric pollutants in the local atmosphere. Overall, these mixing
123 conditions are mostly controlled by the seasonal variation in the height of the local
124 boundary layer (Carballo-Chaves et al., 2020). Therefore, the analysis of stable isotopes in
125 precipitation and its chemistry can provide valuable insights of hydrometeorological
126 conditions and rainfall generation processes controlling the nitrogen wet deposition
127 mechanisms. We propose that $\delta^{15}N-NO_3^-$ and $\delta^{18}O-NO_3^-$ values in atmospheric nitrate are
128 not only controlled by temporal nitrogen emission source changes and reaction chemistry
129 processes, but also by the proportions of convective versus stratiform rainfall.

130   Here, we present a unique dataset of the water and nitrate stable isotope
131 composition in precipitation in a tropical urban atmosphere of Costa Rica. Based on these
132 isotope datasets and other chemical information, this contribution addresses the following
133 research questions: i) What are the sources of atmospheric nitrogen in the main urban

134 atmosphere of Costa Rica, ii) What are the atmospheric processes influencing the temporal
135 variability of atmospheric nitrate), iii) How do the different rainfall generation processes
136 (i.e., convective vs. stratiform precipitation) affect the wet deposition of atmospheric
137 nitrate? This information is necessary for a better understanding of how nitrogen pollutants
138 from tropical urban environments are introduced in the terrestrial aquatic environments via
139 wet deposition.

140
141 **2. Materials and Methods**

142
143 **2.1. Study area**

144
145 The Central Valley of Costa Rica is characterized by an urban conglomerate, known as the
146 metropolitan area, which comprises the four major cities of Costa Rica (~60% population,
147 ~870 inhabitants per km^2) and includes significant industrial activity. The climate of Costa
148 Rica is influenced by four regional air circulation types: NE trade winds; the latitudinal
149 migration of the Intertropical Convergence Zone (ITCZ); cold continental outbreaks; and
150 the sporadic Caribbean cyclones (Waylen 1996; Hidalgo et al. 2013; Sáenz and Durán-
151 Quesada 2015). In the Central Valley, the dry season ranges from December to April and
152 the wet season ranges from May to November. Between 1982 and 2012, mean annual
153 rainfall was ~2,400 mm, with ~ 85% of the rainfall falling in the wet season (Sánchez
154 Murillo et al. 2016). Strong orographic effects are caused by a NW to SE mountain range
155 (or cordillera) with a maximum elevation of 3,820 m a.s.l., which divides the country into
156 the Caribbean and Pacific slopes, each slope having distinct precipitation and runoff
157 regimes.
158 Overall, the local anthropogenic emissions (e.g., fossil fuel combustion, transportation,
159 industrial activities) mainly control the accumulation of polluted air over this urban area.
160 Transportation is responsible for 66% of fuel consumption and 54% of these emissions.
161 This fuel consumption is dominated by gasoline, with 75% of the vehicles running on this
162 fuel (www.estadonacion.or.cr). However, industrial activities are based on the consumption
163 of other fuels like diesel which has a high sulfur content (3500–4000 ppm; Herrera et al.,
164 2009). Volcanic emissions from nearby volcanoes also contribute to the local SO_2
165 emissions. The volcano's plumes, due to the prevailing wind direction, are transported
166 directly to this region of Costa Rica (Campion et al., 2012).
167   The accumulation of air pollutants is enhanced during the wet season by a reduction
168 in the mixed layer height, which decreases the intensity of the gas mixing dynamics in the
169 local atmospheric boundary layer (Carballo-Chaves et al. 2020; Esquivel-Hernández et al.
170 2015). The chemical composition of precipitation collected in the capital city (San José) is
171 also affected by contributions from these anthropogenic emissions (e.g., NO_x and SO_2)
172 during the wet season (Herrera-Murillo and Rodríguez-Román 2009). However, other
173 remote sources of reactive nitrogen like fertilization-related soil emissions (Hergoualc'h et
174 al. 2008), biomass burning (Fibiger and Hastings, 2016) and lighting NO_x (Schumann and
175 Huntrieser, 2007) are also expected in the Central Valley. In Costa Rica, a land use
176 transition with a simultaneous increase in food production and forest cover was observed in
177 the past years (Lambin and Meyfroidt 2011). For instance, pineapple plantations have
178 proliferated in the lowlands of northern and southern Costa Rica, overtaken coffee to

179 become Costa Rica's second largest agriculture export after bananas (Ingwersen 2012). In
180 2010-2011, the consumption of fertilizers like ammonium nitrate and urea was estimated to
181 be 15 Gg-N/yr and 28 Gg-N/yr, respectively (MEIC 2011). It is also reported that the
182 production of sugarcane in the Pacific region of Costa Rica is based on biomass burning for
183 energy production (Ulloa et al. 2018). Therefore, these NO_x emissions can also be
184 transported to the Central Valley and contribute to the local budget of reactive nitrogen.
185 Regarding the production of NO_x from lighting, lightning is the primary contributor (up to
186 70%) to the total NO_x concentration in the subtropical and tropical free troposphere (Allen
187 et al., 2010; Felix and Murgulet, 2020). Findings in our region indicate that NO_x production
188 per flash is ∼100–250 mol/flash (Bucsela et al. 2010). Besides, under the influence of
189 strong convective activity (e.g., tropical cyclones) up to 1000 flashes/hour were recorded in
190 Costa Rica (Arce-Fernández and Amador, 2020). It is worth mentioning that NO_x
191 emissions from coal combustion can be ruled out for our study site because no coal
192 combustion is reported in Costa Rica.

194 **2.2. Sampling methodology**

196 The sampling site was located at the main campus of Universidad Nacional, Costa Rica
197 (Latitude: 10.005°, Longitude: -84.109°) which is a typical urban site of the Central Valley
198 of Costa Rica. Precipitation samples (N= 111) were collected after 24 hours (i.e., daily
199 basis) on 7:00-9:00 am of each day between August 2018 and November 2019 using a
200 passive collector (Palmex Ltd., Croatia) (Gröning et al. 2012). No samples were collected
201 between December 2018 and April 2019 (dry season). Samples were filtered using 0.45 μm
202 polytetrafluorethylene (PTFE) syringe membranes and divided in two portions: i) 30 mL
203 were stored at dark and frozen conditions (-10°C) until shipment for nitrogen isotopic
204 analysis at the International Atomic Energy Agency (IAEA), ii) 30 mL were stored at dark
205 and cool conditions (5°C) until ion and water isotope analyses at the Stable Isotopes
206 Research Group facilities (Universidad Nacional, Costa Rica). The pH and electrical
207 conductivity were measured after sample collection using a Benchtop Multiparameter
208 Meter Mi-180 (Milwaukee Instruments, USA). To account for the possible contamination
209 from dry deposition, the collector's funnel and the transfer line to the vessel was rinsed
210 with deionized water every day after the samples were collected. Hourly meteorological
211 conditions were registered at the sampling site with a Vantage Pro2 weather station (Davis
212 Instruments, Hayward, CA, USA).

214 **2.3. Laboratory analysis**

216 The concentration of major cations and anions in precipitation samples was analyzed using
217 a Dionex Ion Chromatograph ICS 5000+ (Dionex, CA). The following chemical parameters
218 were quantified: nitrate (NO_3^-), nitrite (NO_2^-), chloride (Cl^-), sulphate (SO_4^{2-}), ammonium
219 (NH_4^+), sodium (Na^+), calcium (Ca^{2+}), potassium (K^+), and magnesium (Mg^{2+}). To assess
220 the quality of our data, the standard operating procedures described by the Global
221 Atmospheric Watch Precipitation Chemistry Programme were followed and the ion balance
222 of each sample was calculated (WMO 2004). For those samples with pH>5, bicarbonate
223 (HCO_3^-) concentration in μeq/L was calculated using the pH and the acid-base equilibrium
224 (WMO 2004):

$$HCO_3^- = \frac{5.10}{10^{(6-pH)}} \qquad (1)$$

Those samples with ion differences outside the range ±20% were flagged and checked for possible contamination issues (N=15). Of these samples, most were related to pH values greater than 6.3 (i.e., carbonated samples) and/or low electrical conductivities (<10 µS/cm). We also checked the nitrate concentration of our samples to see if the maximum nitrate concentration in rainfall reported for the Central Valley was exceeded (up to ~5 mg/L) as these high nitrate concentrations could indicate contamination issues (Herrera-Murillo and Rodríguez-Román 2009). Therefore, two samples were excluded from the data analysis. The detection limits were calculated as follows: NO_3^- (0.3 mg/L, expressed as NO_3^-), Cl^- (0.15 mg/L), SO_4^{2-} (0.2 mg/L), NH_4^+ (0.15 mg/L, expressed as NH_4^+), Na^+ (0.03 mg/L), Ca^{2+} (0.04 mg/L), K^+ (1.0 mg/L), and Mg^{2+} (0.03 mg/L). No nitrite data is reported because it was below the detection limit in all samples (<0.3 mg/L). Hereafter the ion concentrations are expressed in µeq/L.

Stable isotopes analysis of precipitation samples (N=110) was performed using a water isotope analyzer LWIA-45P (Los Gatos Research Inc., USA). The secondary standards were MTW ($\delta^2H = -131.4$ ‰, $\delta^{18}O = -17.0$ ‰), DOW ($\delta^2H = -1.7$ ‰, $\delta^{18}O = -0.2$ ‰), and CAS ($\delta^2H = -64.3$ ‰, $\delta^{18}O = -8.3$ ‰). MTW and DOW standards were used to normalize the results to the VSMOW-SLAP scale. The uncertainty of these international standards is 0.3 ‰ (^2H) and 0.02 ‰ (^{18}O) (IAEA 2017). The CAS standard was used as a quality control and drift control standard. The analytical long-term uncertainty was: ± 0.5 ‰ (1σ) for ^2H and ± 0.1 ‰ (1σ) for ^{18}O. Stable isotope compositions are presented in delta notation δ (‰, per mil), relating the ratios (R) of $^{18}O/^{16}O$ and $^2H/^1H$, relative to Vienna Standard Mean Ocean Water (V-SMOW).

Seventy-six precipitation samples, collected between August 2018 and July 2019, were shipped for nitrogen isotopic analysis ($\delta^{15}N$-NO_3^- and $\delta^{18}O$-NO_3^-) to the Isotope Hydrology Laboratory (IAEA). This laboratory uses a Ti (III) reduction method, which involves a one-step chemical conversion employing $TiCl_3$ to reduce NO_3^- to N_2O gas in septum sample vials (Altabet et al. 2019). The N_2O headspace was measured for ^{15}N and ^{18}O by coupling with a continuous-flow Isotope-Ratio Mass Spectrometer-IRMS (Isoprime 100) and a Trace Gas N2O purification device. The analytical uncertainties were ±0.2‰ and ±0.4‰ for $\delta^{15}N/\delta^{18}O$-$NO_3^-$, respectively. The stable isotope ratios were expressed in delta (δ) and a permil (‰) notation relative to an international standard. Values of $\delta^{15}N$ were reported relative to N_2 in atmospheric air (AIR) and $\delta^{18}O$ values were reported relative to Vienna Standard Mean Ocean Water (VSMOW). The standards used for the analysis were USGS34 (-1.8 ± 0.1 for $\delta^{15}N_{AIR}$ and $+27.9 \pm 0.3$ ‰ for $\delta^{18}O_{VSMOW-SLAP}$), USGS35 ($+2.7 \pm 0.1$ ‰ for $\delta^{15}N_{AIR}$ and $+57.5 \pm 0.3$ ‰ for $\delta^{18}O_{VSMOW-SLAP}$) and IAEA-NO3 ($+4.7 \pm 0.2$ ‰ for $\delta^{15}N_{AIR}$ and $+25.6 \pm 0.4$ ‰ for $\delta^{18}O_{VSMOW-SLAP}$).

2.4 Air mass trajectory analysis

The HYSPLIT (Hybrid Single-Particle Lagrangian Integrated Trajectory) model was used to calculate the preferential transport pathways followed by the air masses that arrived at

the Central Valley (Stein et al. 2015; Rolph et al. 2017). Air parcel back trajectories were estimated on 72 hours basis. The time frame was selected based on the lifetime of NO_x in the boundary layer which is generally less than two days and due to the proximity of the Caribbean Sea and the Pacific Ocean (Fang et al. 2011; Sánchez-Murillo et al. 2016). Each trajectory was calculated using NOAA's meteorological data files (GDAS, global data assimilation system: 2006-present; 0.5° (~50 km resolution) (Su et al. 2015). The ending altitude of air masses was set to the mean elevation of the Central Valley of Costa Rica (~1,100 m a.s.l.). Trajectory analyses ending times at the Central Valley were set to 12:00 UTC, which correspond to a local time of 06:00 a.m. in Costa Rica

2.5 Data analysis

Pearson's correlation analysis was performed to evaluate potential relationships between ion concentrations and isotopic values of precipitation and atmospheric nitrate. Statistical analyses were done using SigmaPlot software 11.0. An α level of 0.05 was inferred as indicating significance. Kruskal-Wallis test was performed for nitrate concentration and isotopic values in precipitation to identify the differences between Caribbean and Pacific air masses. Simple linear regression analysis was used to construct the local meteoric water line (LMWL) and the $\delta^{15}N\text{-}NO_3^-$ and the $\delta^{18}O\text{-}NO_3^-$ dual plot for atmospheric nitrate.

To calculate the average stratiform rainfall fraction contributing to each precipitation event, the following statistically significant relationship of stratiform rainfall area fractions, F_{st} (5°×5° box) and $\delta^{18}O$ values estimated for our study site was applied:

$$\delta^{18}O - H_2O = 18.4 x F_{st} - 49.7\text{‰} \ (E1)$$

Convective/stratiform classification data was based on Ku-band Precipitation Radar (KuPR) product of GPM (Global Precipitation Measurement) Core Observatory (Version 5, Level 2, https://pmm.nasa.gov/GPM), which is a successor of the TRMM Precipitation Radar. The above-mentioned relationship was estimated for the sampling period 2013–2017; (N=929; R^2=0.32, p<0.05) which comprises five-year precipitation data collected under varying climatic conditions (e.g., warm/cold ENSO episodes). Therefore, it can provide good approximations of stratiform rainfall fractions contributing to the precipitation collected during our sampling period (Munksgaard et al., 2019).

To quantify the equilibrium fractionation of nitrogen isotopes during NO_x oxidation and HNO_3 formation, we applied the mathematical formulations described by Felix and Murgulet (2020). In brief, the overall $\delta^{15}N$ fractionation (ϵ_N) can be predicted using the following isotope balance relationship:

$$\varepsilon_N = f_{OH} x \varepsilon_{OH} + f_{N2O5} x \varepsilon_{N2O5} \ (E2)$$

where f_{OH} is the fraction of ·OH pathway and f_{N2O5} is fraction of the N_2O_5 pathway. The ·OH and N_2O_5 fractions estimated by Alexander et al. (2009) for the tropics were applied in equation 2, namely 87% for the ·OH pathway and 13% for the N_2O_5 pathway. The ϵ_N requires the ambient temperature, NO_2 mixing ratio and the fraction of NO_2 to NO_x ($f_{NO2/NOx}$) for the study site. The average monthly temperature for the Central Valley during the study period was 21.4±0.5 °C (1σ). The average NO_2 mixing ratio of 38.6 ppbv

7

reported by Herrera et al. (2009) and Herrera-Murillo et al. (2011) was included in the calculations. However, no NO_x speciation is available for the Central Valley. Therefore, it is not possible to calculate the $f_{NO2/NOx}$ for our study site. It is reported that $f_{NO2/NOx}$ values may be in the range 0.20 to 0.75 in some urban areas (Rao and George, 2014; Richmond-Bryant et al., 2017). Nevertheless, it is expected that the $f_{NO2/NOx}$ ratios in our study site to be high because the ·OH pathway dominates in the tropical atmospheres (Alexander et al., 2009). Therefore, the calculations of ε_N were performed for $f_{NO2/NOx}$ ratios in the range 0.75 to 1.00 (N=6 corresponding to 0.05 ratio increments). Thus, we report the average ε_N value and the estimated error as the standard deviation of dataset. The temperature-dependent isotope effects on the fractionation factors, namely $^{15}\alpha_{NO2/NO}$ and $^{15}\alpha_{N2O5/NO}$, were estimated using the equations reported by Walters and Michalski (2015).

Overall, the $\delta^{18}O\text{-}NO_3^-$ values are determined by the reactions that produce NO_3^- (R1-R6) and not the original source of NO_x (Hastings and Sigman 2003; Shrestha et al. 2013). The $\delta^{18}O\text{-}NO_3^-$ values reflect the transfer from O_3 (R1 and R4) during cycling with NO_x ($\delta^{18}O$ in O_3 falls in the range ~+80 - +120‰ vs. VSMOW) and the reaction of NO_2 with ·OH (R3) that also contributes to the oxygen isotope of NO_3^- (Morin et al., 2008; Savarino et al., 2008; Michalski et al. 2011). However, the peroxy radical (RO_2) oxidation pathway has been suggested as a competing pathway leading to lower than usual $\delta^{18}O\text{-}NO_3^-$ values (Fang et al. 2011):

$$NO + RO_2 \rightarrow NO_2 + RO \ (R7)$$
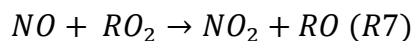
To account for this competing reaction, Felix and Murgulet (2020) also describe a mathematical approach to determine the % O_3 and RO_2 competing daytime oxidation reactions (R1) and (R7) that occur before subsequent ·OH oxidation reaction (R3). However, it is not possible to perform these calculations for our study area due to the complex atmospheric chemistry prevailing in our tropical environment. The Central American volcanoes are known to be important emitters of halogen emissions (e.g., BrO and ClO) in our region. There is evidence that these emissions can strongly interact with ozone and species like H_XO_Y and NO_X and impact the local atmospheric chemistry (de Moor et al. 2013; Rüdiger et al., 2020). Additionally, the local atmosphere of the Central Valley is under the strong influence of biogenic emissions like biogenic volatile organic hydrocarbons (BVOC; Esquivel-Hernández et al., 2011). Therefore, the air chemistry in our tropical atmosphere is highly sensitive because of the high solar radiation and concentrations of water vapor with plentiful BVOC emissions and the subsequent impact of the production of secondary organic aerosols (SOA) via the $RO_2 + HO_2$ pathway (Santos et al., 2018; Yañez-Serrano et al., 2020). Therefore, these additional chemical pathways associated to the halogen and organic reactive species should be accounted to perform a quantitative analysis of the $\delta^{18}O\text{-}NO_3^-$ variations for our study site (i.e., the % O_3 vs. RO_2 participating in the daytime oxidation). However, these calculations are outside the scope of our work and more investigation is needed on this matter.

2.6 Stable isotope mixing model

We applied the stable isotope mixing model from the R package Simmr to partition relative nitrogen sources for our study region using a Bayesian statistical framework based on a Gaussian likelihood (Parnell and Inger, 2016). Based on the identified NOx emissions

sources in our region, the following NO_x endmembers were included in the mixing model: lightning, fossil fuels (i.e., gasoline and diesel), soils emissions from biogenic activity, and biomass burning. The corresponding $\delta^{15}N\text{-}NO_3^-$ and deviations of these sources are: +0.5 ± 0.9‰, -3 ± 6‰, -13 ± 7‰, -35 ± 10‰, and +1 ± 4‰, respectively (Elliot et al., 2019; Felix and Elliot, 2014; Felix and Murgulet, 2020; Fibiger et al., 2014; Fibiger and Hastings, 2016; Heaton, 1987; Heaton, 1990; Li and Wang, 2008; Walters et al., 2015; Yu and Elliot, 2017).

3. Results

3.1 Precipitation chemical and isotopic characteristics

Data of ion concentrations and isotope compositions (water and nitrate) in precipitation are summarized in Table 1. Even though the study site is situated within an urban conglomerate, the average pH of 5.72 measured in the precipitation was not lower than the global average of 5.7 for pollution-free areas (Balestrini et al. 2016). The major anion was sulphate, contributing with ~18% to the total ion concentration, whereas calcium was the major cation, with a contribution of ~11% to the total. As for nitrate, the $25^{th}\text{-}75^{th}$ percentil range was between 14.5 and 26.6 µeq/L for the entire dataset. Some values (N=9) fell outside this range with values up to 85.5 µeq/L. The average contribution of nitrate to the total ion concentration was ~ 8%. The average depositon flux of nitrate for the study site, based on the daily precipitation amounts and the daily nitrate concentrations, was calculated as 4.5 mg $N\text{-}NO_3^-/m^2$ day (range: 0.2 – 16.7 mg $N\text{-}NO_3^-/m^2$ day).

The average oxygen isotope composition ($\delta^{18}O\text{-}H_2O$) in precipitation was -8.61 ± 3.45‰ (range: -20.38‰ – -0.52‰, Table 1), whereas the average $\delta^2H\text{-}H_2O$ was -59.37 ± 28.21‰ (range: -1.86‰ – -153.35‰, Table 1). Based on these isotope data, the LMWL was constructed (Figure 1A and 1B). The following meteoric water line (LMWL) was calculated for the study site: $\delta^2H\text{-}H_2O=8.05\cdot\delta^{18}O\text{-}H_2O+9.68‰$ (p<0.001; R^2=0.97, Figure 1A). The slope and intercept parameters of the LMWL are consistent with those of the GMWL and with the historical data reported for the Central Valley of Costa Rica (Munksgaard et al. 2019; Craig 1961; Sánchez-Murillo et al. 2013). The relationships between selected chemical and isotopic parameters in precipitation are shown in Figure 2.

3.2 Temporal variations of nitrate, $\delta^{18}O\text{-}H_2O$, $\delta^{15}N\text{-}NO_3^-$, and $\delta^{18}O\text{-}NO_3^-$

The wet/dry-season precipitation pattern of the Central Valley, with two rain maxima in May-June and in September-October, is shown in Figure 3A. Average daily precipitation during the wet season was 18 mm/day, with values up to 86 mm/day. The overall trend in the nitrate concentrations (µeq/L) shown in Figure 3B indicate that during those rain maxima? periods, higher nitrate values were recorded (up to 85.5 µeq/L), particularly after a long dry period. This characteristic was more visible during the transition periods (Apr-May and Nov-Dec).

As for $\delta^{18}O\text{-}H_2O$, the strongest depletion in ^{18}O registered during the rainiest periods, for instance in October 2018 (up to -20.38‰, Figure 3C), are likely the result of the passage of the ITCZ over Costa Rica and higher stratiform fractions, whereas higher $\delta^{18}O\text{-}H_2O$ values were registered when convective rain exceeded stratiform precipitation during the transition

seasons and the Mid-Summer Drought (MSD) (Munksgaard et al. 2019; Sánchez-Murillo et al. 2019). The variation in $\delta^{15}N$-NO_3^- shown in Figure 3D was systematic along the first study period (August 2018-November 2018). A decrease in $\delta^{15}N$-NO_3^- was observed toward the end of the rainy period in August 2018-October 2018 (up to -3.81‰), whereas an increasing trend was registered at the beginning of rainy period in April-July 2019 (up to +4.09‰). For the period August-November 2019, random variations in the range -1.6‰ – +5.2‰ were observed. As for $\delta^{18}O$-NO_3^- (Figure 3E), these values did not follow the trend observed in $\delta^{15}N$-NO_3. For instance, the strongest enrichment in ^{18}O-NO_3 were recorded during the rainiest periods (October and May), with values up to +65.3‰. The lower isotopic values were registered during the transition seasons and the MSD (up to +33.7‰). Between August 2019 and November 2019, the $\delta^{18}O$-NO_3^- showed relatively smaller variations (+54.9 ± 3.4‰).

3.3 Nitrate wet deposition

Based on the HYSPLIT trajectory analyses, air masses that arrived at the Central Valley of Costa Rica mostly came from the Caribbean Sea (N=80, 73%), whereas the moisture contribution from the Pacific Ocean was less common (N=30, 27%, Figure 4A). At $p<0.001$, the average stratiform fraction calculated for the Caribbean samples (0.403±0.158, 1σ) was lower than the average stratiform fraction of the Pacific samples (0.522±0.147, 1σ).
As shown in Figure 2, a poor correlation between $\delta^{18}O$-H_2O and NO_3^- was preliminary found for the whole dataset (r=0.248, p>0.05). However, if the air mass pathways of the precipitation events are considered and the data are further split into the two groups, namely Caribbean and Pacific, differences were found between the $\delta^{18}O$-H_2O values and NO_3^- concentrations (Figure 5A and 5B). The average $\delta^{18}O$-H_2O value of the Caribbean samples was significant higher than the corresponding value of the Pacific samples (-8.02‰ and -10.51‰, p<0.001). As for the NO_3^- concentrations, the average concentration of NO_3^- in the Caribbean samples was higher than the corresponding value in the Pacific samples (22.5 µeq/L and 17.8 µeq/L, p=0.068). The average $\delta^{15}N$-NO_3^- value in the Pacific samples (+1.6‰) was higher than the corresponding value (+0.5 ‰) in the Caribbean samples (p=0.064 Figure 5C). No correlation (r=-0.052, p=0.654, N = 76) was found between $\delta^{15}N$-NO_3^- and $\delta^{18}O$-NO_3^- (Figure 6A). $\delta^{15}N$-NO_3^- values in nitrate, resulted in a normal distribution (Figure 6B, p>0.05), whereas $\delta^{18}O$-NO_3^- in nitrate showed a depleted and slightly left-skewed distribution (Figure 6C, p<0.05). For the Caribbean samples, we found a direct proportional relationship between the $\delta^{18}O$-NO_3^- and the nitrate concentration (r=0.288, p<0.05; N=59; Figure 6A). However, no relationship was found between $\delta^{15}N$-NO_3^- and nitrate concentration (p>0.05). For the Pacific samples, in turn, no proportional relationship between $\delta^{18}O$-NO_3^- and the nitrate concentration was found (p>0.05) but a direct proportional relationship between $\delta^{15}N$-NO_3^- and the nitrate concentration (r=0.481, p=0.05, N=17, Figure 6A).

3.3 NO_x emission sources and fractionation processes

To account for the ^{15}N fractionation during the oxidation of the NO_x emissions, we calculated a NO_x to HNO_3 ε value of 8.89 ± 4.04‰ and corrected our $\delta^{15}N$-NO_3^- values for

potential fractionation effects before applying the Bayesian model to partition the relative nitrogen sources for our study region. The ε values varied from 14.31 ($f_{NO2/NOx}$ = 0.75) and 3.51 ($f_{NO2/NOx}$ = 1.00). Overall, this ε value is somewhat higher compared to the corresponding value of ~5.6‰ reported by Felix and Murgulet (2020). For the Caribbean samples, the contributions of nitrogen sources were 42.7 ± 6.2% (biomass burning), 0.8 ± 0.4% (soils biogenic emissions), 15.8 ± 6.3% (gasoline), 2.1 ± 1.2% (diesel), and 38.6 ± 6.3% (lightning). The corresponding contributions for the Pacific samples were 46.0 ± 13.9%, 1.6 ± 1.0%, 12.3 ± 9.1%, 3.6 ± 2.7%, and 36.5 ± 13.8%, respectively (Figure 7).

4. Discussion

The available data on precipitation chemistry for the Central Valley of Costa Rica are scarce. Two previous research efforts reported that most samples showed pH values between 4.0 and 5.6, and only 26% of them were basic (pH>7) (Herrera-Murillo and Rodríguez-Román 2009; Herrera et al. 2009). As for our study, the pH range was relatively higher with most samples falling between 4.9 and 6.3 and only ~13% of these samples had pH values greater than 7. Overall, most low pH values were found in September and October when the influence of the ITCZ intensifies precipitation but also reduces wind speed across the Central Valley, which in turns enhances the wet deposition of NO_3^- and SO_4^{-2} and acidifies the precipitation (Esquivel-Hernández et al. 2015). As for the ion composition, our data agree well with the available information that reported SO_4^{2-} among the most abundant ions, but also a high correlation with NO_3^- and NH_4^+ indicating a common anthropogenic origin (Herrera et al. 2009). At other tropical locations, like São Pablo, Brazil and the Indo-Gangetic Plains in India, authors also reported similar ion species in the local precipitation (Martins et al. 2019; Tiwari et al. 2019). Due to its location in the narrow land bridge of Central America and proximity to the Caribbean Sea and the Pacific Ocean (Figure 4), some contributions from sea salt could be expected in the precipitation of the Central Valley (Kajino and Aikawa 2015; Vet et al. 2014). However, a predominant contribution from Non-Sea-Salt sulphate (NSS-SO_4^{2-}) was found in the precipitation of our study site with an average percentage of 93±5% (range: 76 – 100%). Therefore, it seems that the average contribution is mainly produced from natural and anthropogenic sources (e.g., SO_2 from volcanoes, industrial and traffic emissions). The correlation between NO_3^- and SO_4^{2-} (r=0.270; p<0.05) also suggests the influence of a common anthropogenic source like fossil fuels (SO_2, NO_x, Figure 2). Besides, the photochemical oxidation in the atmosphere may also control and enhance the nitrogen wet deposition in the urban conglomerate (Shresta et al. 2013; Xiao 2016; Decina et al. 2019; Martins et al. 2019). As ammonia (NH_3) plays an important role as it is the main neutralizing gas for acidic compounds like HNO_3 and H_2SO_4 in the atmosphere, the correlation between NH_4^+ and SO_4^{2-} (r=0.525, p<0.001) is also an indication of common anthropogenic sources of NH_3 and SO_2.

It was possible to separate the convective rain events, typically more enriched in ^{18}O, from the stratiform ones using the relationship between $\delta^{18}O$-H_2O and stratiform fraction (Equation 1). Overall, the relationship between precipitation amount and $\delta^{18}O$-H_2O showed that the "amount effect" is in convective precipitation than in the stratiform rainfall (Dansgaard 1964; Tharammal et al. 2017). For the Caribbean samples, a correlation was indeed found between P (precipitation amount) and $\delta^{18}O$-H_2O and a correlation between P

501 and NO_3^- was also verified. On the other hand, no "amount effect" was found between P,
502 $\delta^{18}O$-H_2O, and NO_3^- in the Pacific samples. Therefore, the wet deposition of nitrate seems
503 to be affected by the rainfall generation processes, namely by the formation spatial-limited
504 and high-intensity convective precipitation or widespread and lower-intensity stratiform
505 rainfall (Aggarwal et al. 2016; Galewsky et al. 2016). When the formation of precipitation
506 is mostly controlled by deep convection and air masses arriving from the Caribbean Sea
507 (i.e., high $\delta^{18}O$-H_2O values), relatively higher concentrations of nitrate were found in the
508 precipitation samples due to increased dilution effect (Lacaux et al., 1992) (Figure 5B).
509 This characteristic was more evident at the beginning of the rainiest periods, namely
510 August 2018, May 2019, July 2019, and August 2019 (Figure 3C), when high-intensity
511 precipitation events of short duration were recorded. With regard the Pacific samples, as the
512 wet season advances (September-November), the contribution of frontal and continuous
513 precipitation events from Pacific air masses increased (Sánchez-Murillo et al. 2016;
514 Munksgaard et al. 2019). These higher stratiform factions in rainfall (i.e., low $\delta^{18}O$-H_2O
515 values) was related to the scavenging of smaller amounts of NO_3^- due to the "wash-out"
516 effect, namely the decrease in the concentration of solutes in precipitation after succeeding
517 precipitation events (Kajino and Aikawa 2015; Guo et al. 2016).
518 $^{15}N/^{14}N$ and $^{18}O/^{16}O$ ratios are impacted by source changes and variations in
519 reaction chemistry prior to NO_3^- deposition (Michalski et al. 2011; Hastings and Sigman,
520 2003). Our findings show that these source changes and chemistry variations can be
521 inferred from the rainfall generation processes, namely the convective vs. stratiform
522 fractions. The higher relative contribution of gasoline NOx emissions found in the
523 Caribbean samples seems to reflect the oxidation of these emissions and the removal via
524 high-intensity convective precipitation in the Central Valley. There is also a higher relative
525 contribution of NO_x lightning in these samples, probably due to the convective activity
526 formed over the Caribbean Sea (Altieri et al., 2013). In turn, $\delta^{15}N$-NO_3^- variations in Pacific
527 samples are related to the frontal, continuous and wide-spread character of stratiform
528 clouds and higher contributions of diesel, biomass burning, and soils biogenic emissions.
529 The latter emissions are mostly transported from the Pacific and Caribbean lowlands to the
530 Central Valley, where cultivated areas are spatially distributed (Figure 4B). The relatively
531 high concentration of K^+ in our samples (with an average concentration of 24.6 µeq/L,
532 Table 1) also seems to point out the contribution of biomass burning to nitrate wet
533 deposition (Vieira-Filho et al. 2013). Due to the predominant influence of air masses
534 travelling over the Caribbean Sea on our study site, the regional transport of NO_x
535 emissions, for example from ships sailing to or from the Panama Canal and marine
536 aerosols, cannot be excluded (Wankel et al., 2010; Gobel et al., 2013; Beyn et al. 2015).
537 We found some nitrate samples enriched ^{15}N that may be related to the input of emissions
538 from ships (Figure 3).
539 Regarding our $\delta^{18}O$-NO_3^- data, the correlation found between $\delta^{18}O$-NO_3^- and NO_3^-
540 (r=0.265; p<0.05) could reflect the atmospheric processing of NO_x prior to deposition of
541 NO_3^-. Overall, these isotope values provide information about the oxygen transfer to NO_x
542 due to ·OH formation pathway when the convective fractions I rainfall increase.
543 Nevertheless, there are also relatively low $\delta^{18}O$-NO_3^- values (up to +33.7‰) in our samples
544 that may be related to the RO_2 oxidation pathway (R7). Generally, in convective clouds like
545 cumulus or cumulonimbus, the condensation particles are formed near the cloud base and
546 grow as they are lifted in strong updrafts (Aggarwal et al. 2016; Galewsky et al. 2016;

547 Schumacher and Houze, 2003). As recognized by Felix and Murgulet (2020), these strong
548 vertical motions can effectively transport $\cdot OH$ and RO_2 to the upper troposphere and then
549 react with lightning NO_x, increasing the probability of NO_x oxidation via the RO_2 pathway.
550 Nevertheless, unlike convective clouds, in stratiform clouds the vertical air motions are
551 weak and the upward air velocity is low (Aggarwal et al. 2016) and the NO_x oxidation via
552 RO_2 may be less important. The less variation observed in $\delta^{18}O\text{-}NO_3^-$ values during the
553 rainiest period (August-November) may indicate a decrease in the convective activity in the
554 Central Valley.

5. Conclusions

558 The stable isotope data in precipitation and atmospheric nitrate described here provide a
559 novel contribution to the study of wet deposition processes and the origin of inorganic
560 nitrogen loadings in tropical regions like Costa Rica. Our results reveal that the ^{15}N and ^{18}O
561 fractionation via photochemical oxidation and the rainfall generation processes (i.e.,
562 convective and stratiform rainfall) inform about the atmospheric oxidation pathways and
563 the nitrate wet deposition processes in the local urban atmosphere. Overall, $\delta^{18}O\text{-}NO_3^-$
564 values reflect the $\cdot OH$ and RO_2 oxidation pathways when convective rainfall fractions from
565 the Caribbean Sea predominated (i.e., small-scale systems ~1-2 km and high intensity
566 precipitation). In turn, $\delta^{15}N\text{-}NO_3^-$ values, corrected for potential ^{15}N fractionation effects,
567 indicate higher contributions from diesel, biomass burning, and soils biogenic emissions
568 when stratiform rainfall fractions from the Pacific Ocean dominated (i.e., large scale ~100
569 km and low intensity precipitation). Air mass trajectory analysis also supports the possible
570 transport of NO_x emissions from cultivated areas from the Caribbean and Pacific lowlands
571 to the Central Valley.
572   These results highlight the advantage of combining water and nitrogen stable
573 isotopes with atmospheric chemistry and hydrometeorology to study the wet deposition of
574 secondary atmospheric pollutants like nitrate. Given the recent advances in the modeling
575 approaches to simulate atmospheric deposition, the consolidation of a wet deposition
576 network in the Caribbean and Pacific regions of Costa Rica could allow the simulation of
577 distribution maps of nitrogen isotopes in precipitation as a potential source of nitrogen
578 pollution in water systems. Besides, the incorporation of other tracers like $\delta^{34}S$ in
579 atmospheric sulphate and $\Delta^{17}O$ in atmospheric nitrate could also improve the understanding
580 of the fundamental chemical processes that control the wet deposition of nitrogen and its
581 isotopic variability. In this same regard, these new studies could also examine how daytime
582 nitrate wet deposition differ from that occurring at night which in turn is related to how the
583 different photochemical reactions control the NO_x atmospheric oxidation. However, these
584 studies need to account for other oxidations pathways (e.g., BrO and SOA) to determinate,
585 for instance, the % O_3 and RO_2 competing daytime oxidation reactions.

Declarations

589   - *Ethics approval and consent to participate*
590 Not applicable

592   - *Consent for publication*

Not applicable

6. References

Aggarwal PK, Romatschke U, Araguas-Araguas L, Belachew D, Longstaffe FJ (2016)
Proportions of convective and stratiform precipitation revealed in water isotope ratios. Nat
Geosci 9:624-629. https://doi.org/10.1038/ngeo2739

Alexander B, Hastings MG, Allman DJ, Dachs J., Thornton JA, Kunasek SA (2009)
Quantifying atmospheric nitrate formation pathways based on a global model of the oxygen
isotopic composition ($\Delta^{17}O$) of atmospheric nitrate. Atmos Chem Phys 9:5043-5056.
https://doi.org/10.5194/acp-9-5043-2009

Allen D, Pickering K, Duncan B, Damon M (2010) Impact of lightning NO emissions
on North American photochemistry as determined using the Global Modeling Initiative
(GMI) model. J. Geophys. Res. Atmos. 115:1-24. https://doi.org/10.1029/2010JD014062.

Altabet M, Wassenaar L, Douence C, Roy R (2019) A Ti (III) Reduction Method for One-
Step Conversion of Seawater and Freshwater Nitrate to N_2O for Stable Isotopic Analysis of
$^{15}N/^{14}N, ^{18}O/^{16}O$ and $^{17}O/^{16}O$. Rapid Commun Mass Sp 33:1227-1239.
https://doi.org/10.1002/rcm.8454

Altieri KE, Hastings, MG, Gobel AR, Peters AJ, Sigman DM (2013) Isotopic composition
of rainwater nitrate at bermuda: the influence of air mass 179 source and chemistry in the

639 marine boundary layer. J. Geophys. Res. Atmos. 180:118.
640 https://doi.org/10.1002/jgrd.50829
641
642 Andreae MO, Talbot RW, Berresheim H, Beecher KM (1990) Precipitation Chemistry in
643 Central Amazonia. J Geophys Res 95:16987-16999.
644 https://doi.org/10.1029/JD095iD10p16987
645 Arce-Fernández D, Amador JA (2020) Actividad Eléctrica Asociada al Huracán Otto
646 (2016) en el Mar Caribe y en el Corredor Seco Centroamericano. Rev Bras Meteorol
647 131:250-261. http://dx.doi.org/10.1590/0102-77863540064
648 Balestrini R, Delconte CA, Sacchi E, Wilson AM, Williams MW, Cristofanelli P, Putero D
649 (2016) Wet deposition at the base of Mt Everest: Seasonal evolution of the chemistry and
650 isotopic composition. Atmos Environ 146:100-112.
651 https://doi.org/10.1016/j.atmosenv.2016.08.056
652
653 Beyn F, Matthias V, Aulinger A, Dähnke K (2015) Do N-isotopes in atmospheric nitrate
654 deposition reflect air pollution levels? Atmos Environ 107:281-288.
655 https://doi.org/10.1016/j.atmosenv.2015.02.057
656
657 Bucsela EJ, Pickering KE, Huntemann TL, Cohen RC, Perring A, Gleason JF, Blakeslee
658 RJ, Albrecht RI, Holzworth R, Cipriani JP, Vargas-Navarro D, Mora-Segura I, Pacheco-
659 Hernández A, Laporte-Molina S (2010) Lightning‐generated NOx seen by the Ozone
660 MonitoringInstrument during NASA's Tropical Composition, Cloud and Climate Coupling
661 Experiment (TC^4). J Geophys Res 115:1-15. https://doi.org/10.1029/2009JD013118
662
663 Campion R, Martínez-Cruz M, Lecocq T, Caudron C, Pacheco J, Pinardi G, Hermans C,
664 Carn S, Bernard A (2012) Space- and ground-based measurements of sulphur dioxide
665 emissions from Turrialba Volcano (Costa Rica). Bull Volcanol 74:1757-1770.
666 https://doi.org/10.1007/s00445-012-0631-z
667
668 Carballo-Chaves K, Villalobos-Forbes M, Esquivel-Hernández G, Sánchez-Murillo R
669 (2020) Isotope composition of carbon dioxide and methane in a tropical urban atmosphere.
670 Isotopes Environ Health Stud. https://doi.org/10.1080/10256016.2020.1803855
671
672 Craig H (1961) Isotopic variations in meteoric waters. Science 133:1702-1703.
673 https://doi.org/10.1126/science.133.3465.1702
674
675 Dansgaard, W (1964) Stable isotopes in precipitation. Tellus 16:436-468.
676 https://doi.org/10.1111/j.2153-3490.1964.tb00181.x
677
678 de Moor JM, Fischer TP, Sharp ZD, King PL, Wilke M, Botcharnikov RE, Cottrell E,
679 Zelenski M, Marty B, Klimm K, Rivard C, Ayalew D, Ramírez C, Kelley KA (2013)
680 Sulfur degassing at Erta Ale (Ethiopia) and Masaya (Nicaragua) volcanoes: Implications
681 for degassing processes and oxygen fugacities of basaltic systems. Geochem Geophys
682 Geosyst 14:4076-4108. https://doi.org/10.1002/ggge.20255
683

Decina SM, Hutyra LR, Templer PH (2019) Hotspots of nitrogen deposition in the world's urban areas: a global data synthesis. Front Ecol Environ 18:92-100. https://doi.org/10.1002/fee.2143

Durán-Quesada AM, Gimeno L, Amador J (2017) Role of moisture transport for Central American precipitation. Earth Syst Dynam 8:147-161. https://doi.org/10.5194/esd-8-147-2017

Elliot EM, Yu Z, Cole AS, Coughlin JG (2019) Isotopic advances in understanding reactive nitrogen deposition and atmospheric processing. Sci Total Environ 662:393-403. https://doi.org/10.1016/j.scitotenv.2018.12.177

Esquivel-Hernández G, Madrigal-Carballo S, Alfaro-Solís R, Sibaja-Brenes JP, Valdés-González J (2011) First Measurements of Biogenic Hydrocarbons in Air in a Tropical Cloudy Forest, Monteverde, Costa Rica. J Chem Chem Eng 5:1097-1106. https://doi.org/10.1016/253953274

Esquivel-Hernández G, Villalobos-Forbes M, Sánchez-Murillo R, Birkel C, Valdés-González J, Boll J (2015) Near surface carbon dioxide and methane in urban areas of Costa Rica. Open J Air Pollut 4:1-16. https://doi.org/10.4236/ojap.2015.44018

Fang YT, Koba K, Wang XM, Wen DZ, Li J, Takebayashi Y, Liu XY, Yoh M (2011) Anthropogenic imprints on nitrogen and oxygen isotopic composition of precipitation nitrate in a nitrogen-polluted city in Southern China. Atmos Chem Phys 11:1313-1325. https://doi.org/10.5194/acp-11-1313-2011

Felix JD, Elliot EM, Gay DA (2017) Spatial and temporal patterns of nitrogen isotopic composition of ammonia at U.S. ammonia monitoring network sites. Atmos Environ 150:434-442. https://doi.org/10.1016/j.atmosenv.2016.11.039

Felix JD, Elliott EM (2014) Isotopic composition of passively collected nitrogen dioxide emissions: vehicle, soil, and livestock source signatures. Atmos. Environ. 92:359-366. https://doi.org/10.1016/j.atmosenv.2014.04.005

Felix JD, Murgulet D (2020) Nitrate isotopic composition of sequential Hurricane Harvey wet deposition: Low latitude NOx sources and oxidation chemistry. Atmos Environ 238:1-9. https://doi.org/10.1016/j.atmosenv.2020.117748Felix JD, Elliott EM, Shaw SL (2012) The isotopic composition of coal-fired power plant NOx: The influence of emission controls and implications for global emission inventories. Environ Sci Technol 46:3528-3535. https://doi.org/10.1021/es203355v.

Fibiger DL, Hastings, MG, Lew AF, Peltier RE (2014) Collection of NO and NO_2 for isotopic analysis of NO_x emissions. Anal. Chem. 86:12115-12121. https://doi.org/10.1021/ac502968e

Fibiger DL, Hastings MG (2016) First measurements of the nitrogen isotopic 147 composition of NOx from biomass burning. Environ. Sci. Technol. 50:11569-11574.

729   https://doi.org/10.1021/acs.est.6b03510

731   Fowler D, Coyle M, Skiba U, Sutton MA, Cape JN, Reis S, Sheppard LJ, Jenkins A,
732   Grizzetti B, Galloway JN, Vitousek P, Leach A, Bouwman AF, Butterbach-Bahl K,
733   Dentener F, Stevenson D, Amann M, Voss M (2013) The global nitrogen cycle in the
734   twenty-first century. Phil Trans R Soc B Sci 368:1-13.
735   https://doi.org/10.1098/rstb.2013.0164

737   Galewsky J, Steen-Larsen HC, Field RD, Worden J, Risi C, Schneider M (2016) Stable
738   isotopes in atmospheric water vapor and applications to the hydrologic cycle. Rev Geophys
739   54:809-865. https://doi.org/10.1002/2015RG000512

741   Gobel AR, Altieri KE., Peters AJ, Hastings MG, Sigman DM (2013) Insights into
742   anthropogenic nitrogen deposition to the North Atlantic investigated using the isotopic
743   composition of aerosol and rainwater nitrate. Geophys. Res. Lett. 40:5977-5982.
744   https://doi.org/10.1002/2013GL058167

746   Gröning MH, Lutz O, Roller-Lutz Z, Kralik M, Gourcy L, Pöltenstein L (2012) A simple
747   rain collector preventing water re-evaporation dedicated for $\delta^{18}O$ and δ^2H analysis of
748   cumulative precipitation samples. J Hydrol 448:195-200. .
749   https://doi.org/10.1016/j.jhydrol.2012.04.041

751   Guo LC, Zhang Y, Lin H, Zeng W, Liu T, Xiao J, Rutherford S, You J, Ma W (2016) The
752   washout effects of rainfall on atmospheric particulate pollution in two Chinese cities.
753   Environ Pollut 215:195-202. https://doi.org/10.1016/j.envpol.2016.05.003

755   Harrison RM (2018) Urban atmospheric chemistry: A very special case for study. NPJ
756   Clim Atmos Sci 1:1-5. https://doi.org/10.1038/s41612-017-0010-8

758   Hastings MG, Jarvis JC, Steig EJ (2019) Anthropogenic impacts on nitrogen isotopes of
759   ice-core nitrate. Science 324:1288–1288. https://doi.org/10.1126/science.1170510.

761   Hastings MG, Sigman DM (2003) Isotopic evidence for source changes of nitrate in rain at
762   Bermuda. J Geophys Res 108:1-12. https://doi.org/10.1029/2003JD003789

764   Heaton THE (1987) $^{15}N/^{14}N$ ratios of nitrate and ammonium in rain at Pretoria, South
765   Africa. Atmos. Environ. 21:843-852. https://doi.org/10.1016/0004-6981(87)90080-1

766   Heaton THE (1990) $^{15}N/^{14}N$ ratios of NO_x from vehicle engines and coal-fired power
767   stations. Tellus 42B:304-307. https://doi.org/10.1034/j.1600-0889.1990.00007.x-i1

768   Hergoualc'h K, Skiba U, Harmand JM, Hénault C (2008) Fluxes of greenhouse gases from
769   Andosols under coffee in monoculture or shaded by Inga densiflora in Costa Rica.
770   Biogeochemistry 89:329-345. https://doi.org/ 10.1007/s10533-008-9222-7Herrera-Murillo
771   J, Rodríguez-Román S (2009) Determination of anion concentration in total precipitation
772   samples collected in San José, Costa Rica. Rev Int Contam Ambient 25:65-72 (in Spanish)
773

774 Herrera J, Rodríguez S, Baéz AP (2009) Chemical composition of bulk precipitation in the
775 metropolitan area of Costa Rica, Central America. Atmos Res 94:151-160.
776 https://doi.org/10.1016/j.atmosres.2009.05.004
777
778 Herrera-Murillo J, Rodríguez-Román S, Rojas-Marín JF (2011) Evolución de la
779 contaminación del aire en la ciudad de San José, Costa Rica: 2004-2008. Tecnología en
780 Marcha 24:3-16. https://revistas.tec.ac.cr/index.php/tec_marcha/article/view/74
781
782 Hidalgo HG, Amador JA, Alfaro EJ, Quesada B (2013) Hydrological climate change
783 projections for Central America. J Hydrol 495:94-112.
784 https://doi.org/10.1016/j.jhydrol.2013.05.004
785
786 Ingwersen WW (2012) Life cycle assessment of fresh pineapple from Costa Rica. J Clean
787 Prod 35:152-163. https://doi.org/10.1016/j.jclepro.2012.05.035
788
789 International Atomic Energy Agency (2017) Reference Sheet for VSMOW2 and SLAP2
790 International Measurement Standards. IAEA, Vienna.
791
792 Kajino M, Aikawa M (2005) A model validation study of the washout/rainout contribution
793 of sulfate and nitrate in wet deposition compared with precipitation chemistry data in Japan.
794 Atmos Environ 117:124-134. https://doi.org/10.1016/j.atmosenv.2015.06.042
795
796 Kanakidou M, Myriokefalitakis S, Daskalakis N, Fanourgakis G (2016) Past, present, and
797 future atmospheric nitrogen deposition. J Atmos Sci 73:2039-2047.
798 https://doi.org/10.1175/JAS-D-15-0278.1
799
800 Kendall C, Elliott EM, Wankel SD (2007) Tracing anthropogenic inputs of nitrogen to
801 ecosystems, In Stable Isotopes in Ecology and Environmental Science. Blackwell, 2nd Ed.
802 https://doi.org/10.1002/9780470691854.ch12.
803
804 Konecky BL, Noone DC, Cobb KM (2019) The Influence of Competing Hydroclimate
805 Processes on Stable Isotope Ratios in Tropical Rainfall. Geophys Res Lett 46:1622-1633.
806 https://doi.org/ 10.1029/2018GL080188
807
808 Kurita N (2013) Water isotopic variability in response to mesoscale convective system over
809 the tropical ocean. J Geophys Res-Atmos 118:10376-10390.
810 https://doi.org/10.1002/jgrd.50754
811
812 Lacaux JP, Delmas R, Kouadio G, Cros B, Andreae MO (1992) Precipitation Chemistry in
813 the Mayomb Forest of Equatorial Africa. J Geophys Res 97:6195-6206.
814 https://doi.org/10.1029/91JD00928
815
816 Lambin EF, Meyfroidt P (2011) Global land use change, economic globalization, and the
817 looming land scarcity. Proc Natl Acad Sci U.S.A. 108:3465-3472.
818 https://doi.org/10.1073/pnas.1100480108
819

820 Li D, Wang X (2008) Nitrogen isotopic signature of soil-released nitric oxide (NO) after
821 fertilizer application. Atmos. Environ. 42:4747-4754.
822 https://doi.org/10.1016/j.atmosenv.2008.01.042

823 Liu XY, Xiao HW, Xiao HY, Song W, Sun XC, Zheng XD, Liu CQ, Koba K (2017) Stable
824 isotope analyses of precipitation nitrogen sources in Guiyang, southwestern China. Environ
825 Pollut 230:486-494. https://doi.org/10.1016/j.envpol.2017.06.010
826
827 Martins EH, Nogarotto DC, Mortatti J, Pozza SA (2019) Chemical composition of
828 rainwater in an urban area of the southeast of Brazil. Atmos Pollut Res 10:520-530.
829 https://doi.org/10.1016/j.apr.2018.10.003
830
831 Michalski G, Bhattacharya SK, Mase DF (2011) Oxygen isotope dynamics of atmospheric
832 nitrate and its precursor molecules. In: Baskaran M (ed) Handbook of Environmental
833 Isotope Geochemistry, 1st edn. Springer: Berlin, Germany, pp 613-635.
834
835 Ministry of Economy, Industry and Commerce (2011) Agrochemicals commercialization in
836 Costa Rica. MEIC, Costa Rica. (In Spanish)
837
838 Morin S, Savarino J, Frey MM, Domine F, Jacobi HW, Kaleschke L, Martins JMF (2009)
839 Comprehensive isotopic composition of atmospheric nitrate in the Atlantic Ocean boundary
840 layer from 65°S to 79°N. J. Geophys. Res. 114. https://doi.org/10.1029/2008JD010696
841
842 Munksgaard N, Kurita N, Sánchez-Murillo R, Ahmed N, Araguas L, Balachew DL, Bird
843 M, Chakraborty S, Kien N, Cobb KM, Ellis S, Esquivel-Hernández G, Ganyaglo SY, Gao
844 J, Gastmans D, Kaseke KF, Kebede S, Morales MR, Mueller M, Poh SC, dos Santos V,
845 Shaoneng H, Wang L, Yacobaccio H, Zwart C (2019) Data Descriptor: Tropical daily
846 observations of stable isotope compositions in rainfall and calculated stratiform rainfall
847 fractions. Nature 9:1-18. https://doi.org/10.1038/s41598-019-50973-9
848
849 Parnell A, Inger R (2016). Stable isotope mixing models in R with simmr.
850 Available at: https://cran.r-project.org/web/packages/simmr/vignettes/simmr.
851 html.
852
853 Rao M, George LA (2014) Using the NO_2/NO_x ratio to understand the spatial heterogeneity
854 of secondary pollutant formation capacity in urban atmospheres. AGU Fall Meeting
855 Abstracts. A33F-3265.
856
857 Richmond-Bryant J, Owen RC, Graham S, Snyder M , McDow S, Oakes, M, Kimbrough, S
858 (2017) Estimation of on-road NO2 concentrations, NO_2/NO_x ratios, and related roadway
859 gradients from near-road monitoring data. Air Qual. Atmos. Heal. 10:611-625.
860 https://doi.org/10.1007/s11869-016-0455-7
861
862 Rolph G, Stein A, Stunder B (2017) Real-time Environmental Applications and Display
863 System: READY. Environ Modell Softw 95:210-228.
864 https://doi.org/10.1016/j.envsoft.2017.06.025

865
866 Rüdiger J, Gutmann A, Bobrowski N, Liotta M, de Moor JM, Sander R, Dinger F, Tirpitz
867 JL, Ibarra M, Saballos A, Martínez M, Mendoza E, Ferrufino A, Stix J, Valdés J, Castro
868 JM, and Hoffmann T (2020) Halogen activation in the plume of Masaya volcano: field
869 observations and box model investigations. Atmos Chem Phys 284:1-39.
870 https://doi.org/10.5194/acp-2020-284
871
872 Sáenz F, Durán-Quesada AM (2015) A climatology of low level wind regimes over Central
873 America using a weather type classification approach. Front Earth Sci 3:1-18.
874 https://doi.org/10.3389/feart.2015.00015
875
876 Sánchez-Murillo R, Esquivel-Hernández G, Welsh K, Brooks ES, Boll J, Alfaro-Solís R,
877 Valdés-González J (2013) Spatial and temporal variation of stable isotopes in precipitation
878 across Costa Rica: An analysis of historic GNIP records. Open J Mod Hydrol 3:226-240.
879 https://doi.org/10.4236/ojmh.2013.34027
880
881 Sánchez-Murillo R, Birkel C, Welsh K, Esquivel-Hernández G, Corrales-Salazar J, Boll J,
882 Brooks E, Roupsard O, Sáenz-Rosales O, Katchan I, Arce-Mesén R, Soulsby C, Araguás-
883 Araguás LJ (2015) Key drivers controlling stable isotope variations in daily precipitation of
884 Costa Rica: Caribbean Sea versus Eastern Pacific Ocean moisture sources. Quat Sci Rev
885 131:250-261. https://doi.org/10.1016/j.quascirev.2015.08.028
886
887 Sánchez-Murillo R, Durán-Quesada AM, Birkel C, Boll J, Esquivel-Hernández G (2016)
888 Tropical precipitation anomalies and d-excess evolution during El Niño 2014-16. Hydrol
889 Process 31:1-12. https://doi.org/10.1002/hyp.11088
890
891 Sánchez-Murillo R, Durán-Quesada AM, Esquivel-Hernández G, Rojas-Castillano D,
892 Birkel C, Welsh K, Sánchez-Llull M, Alonso-Hernández CM, Tetzlaff D, Soulsby C, Boll
893 J, Kurita N, Cobb KM (2019) Deciphering key processes controlling rainfall isotopic
894 variability during extreme tropical cyclones. Nat Commun 10:4321.
895 https://doi.org/10.1038/s41467-019-12062-3
896
897 Sánchez-Murillo, R., Esquivel-Hernández, G., Birkel, C., Correa, A., Welsh, K., Durán-
898 Quesada, A.M., Sánchez-Gutiérrez, R., Poca, M. (2020). Tracing Water Sources and Fluxes
899 in a Dynamic Tropical Environment: From Observations to Modeling. Frontiers in Earth
900 Science, 8, 438. https://doi.org/10.3389/feart.2020.571477
901
902 Savarino J, Bhattacharya SK, Morin S M. Baroni, M, Doussin JF (2008) The $NO+O_3$
903 reaction: a triple oxygen isotope perspective on the reaction dynamics and atmospheric
904 implications for the transfer of the ozone isotope anomaly. J Chem Phys 128.
905 https://doi.org/10.1063/1.2917581
906
907 Santos F, Longo K, Guenther A, Kim S, Gu D, Oram D, Forster G, Lee J, Hopkins J, Brito
908 J, Freitas S (2018) Biomass burning emission disturbances of isoprene oxidation in a
909 tropical forest. Atmos Chem Phys 18:12715-12734. https://doi.org/10.5194/acp-18-12715-
910 2018

911 Savarino J, Morin S, Erbland J, Grannec F, Pattey MD, Vicars W, Alexander B, Achterberg
912 EP (2013) Isotopic composition of atmospheric nitrate in a tropical marine boundary layer.
913 PNAS 110:17668-17673. https://doi.org/10.1073/pnas.1216639110

915 Schumacher C, Houze R. A Jr (2003) Stratiform rain in the tropics as seen by the TRMM
916 precipitation radar. J. Climate 16:1739-1756. https://doi.org/10.1175/1520-
917 0442(2003)016<1739:SRITTA>2.0.CO;2

919 Schumann U, Huntrieser H (2007) The global lightning-induced nitrogen oxides source.
920 Atmos. Chem. Phys. 7:3823-3907. https://doi.org/10.5194/acp-7-3823-2007

922 Shrestha S, Nakamura T, Yoneyama Y, Shrestha S, Kazama F (2013) Identification of
923 nitrate sources in rainwater of Kathmandu Valley: a chemical and stable isotopic approach.
924 J Water Environ Tech 11:377-389. https://doi.org/10.2965/jwet.2013.377

926 Song W, Liu XY, Hu CC, Chen GY, Liu XJ, Walters WW, Michalski G, Liu CQ (2021)
927 Important contributions of non-fossil fuel nitrogen oxides emissions. Nature 12:1-7.
928 https://doi.org/10.1038/s41467-020-20356-0

929 Stein AF, Draxler RR, Rolph GD, Stunder BJB, Cohen MD, Ngan F (2015) NOAA's
930 HYSPLIT atmospheric transport and dispersion modeling system. B Am Meteorol Soc
931 96:2059-2077. https://doi.org/10.1175/BAMS-D-14-00110.1

933 Su L, Yuan Z, Fung JCH, Lau AKH (2015) A comparison of HYSPLIT backward
934 trajectories generated from two GDAS datasets. Sci Total Environ 506:527–537.
935 https://doi.org/10.1016/j.scitotenv.2014.11.072

937 Tharammal T, Bala G, Noone D (2017) Impact of deep convection on the isotopic amount
938 effect in tropical precipitation. J Geophys Res – Atmos 122:1505–1523.
939 https://doi.org/10.1002/2016JD025555

941 Tiwari S, Hopke PK, Thimmaiah D, Dumka UC, Srivastaval AK, Bisht DS, Rao PSP,
942 Chate DM, Srivastava MK, Tripathi SN (2019) Nature and Sources of Ionic Species in
943 Precipitation across the Indo-Gangetic Plains, India. Aerosol Air Qual Res 16:943-957.
944 https://doi.org/10.4209/aaqr.2015.06.0423

946 Ulloa A, Camacho D, Arias D, Valverde JC (2018) Analysis of the forest biomass market
947 for energy purposes in the Guanacaste area, Costa Rica. Rev Forestal Mesoam 15:45-52.
948 https://doi.org/10.18845/rfmk.v15i1.3722

950 Vet R, Artz RS, Carou S, Shawa M, Ro CU, Aas W, Baker A, Bowersox VC, Dentener F,
951 Galy-Lacaux C, Hou A, Pienaar JJ, Gillett RM, Forti MC, Gromov S, Hara H, Khodzherm
952 T, Mahowald NM, Nickovic S, Rao PSP, Reid NW (2014) A global assessment of
953 precipitation chemistry and deposition of sulfur, nitrogen, sea salt, base cations, organic
954 acids, acidity and pH, and phosphorus. Atmos Environ 93:3-100.
955 https://doi.org/10.1016/j.atmosenv.2013.10.060

956

957 Vieira-Filho M, Pedrotti JJ, Fornaro A (2013) Assessment of potassium and sodium
958 excesses in rainwater. In: Procedings of the Community Modeling and Analysis Systems
959 (CMAS) Conference, Espirito Santo, Brazil.

960

961 Wallington TJ, Seinfeld JH, Barker JR (2019) 100 years of progress in gas-phase
962 atmospheric chemistry research. Meteorol Monogr 59:1-52.
963 https://doi.org/10.1175/AMSMONOGRAPHS-D-18-0008.1

964

965 Walters WW, Goodwin SR, Michalski G (2015) The nitrogen stable isotope composition
966 (^{15}N) of vehicle emitted NOx. Environ Sci Technol 49:2278–2285.
967 https://doi.org/10.1021/es505580v.

968

969 Wankel SD, Chen Y, Kendall C, Post AF, Paytan A (2010) Sources of aerosol nitrate to the
970 Gulf of Aqaba: evidence from δ^{15}N and δ^{18}O of nitrate and trace metal chemistry. Mar.
971 Chem. 120:90-99. https://doi.org/10.1016/j.marchem.2009.01.013

972

973 Waylen ME (1996) Interannual variability of monthly precipitation in Costa Rica. J Clim
974 9:2606-2613. https://doi.org/10.1175/1520-0442(1996)009<2606:IVOMPI>2.0.CO;2

975

976 World Meteorological Organization (2004) Manual for the GAW Precipitation Chemistry
977 Programme: Guidelines, Data Quality Objectives and Standard Operating Procedures.
978 WMO, USA, New York.

979

980 Xiao HW, Xie LH, Long AM, Ye F, Pan YP, Li DN, Long ZH, Chen L, Xiao HY, Liu CQ
981 (2015) Use of isotopic compositions of nitrate in TSP to identify sources and chemistry in
982 South China Sea. Atmos Environ 109:70-78.
983 https://doi.org/10.1016/j.atmosenv.2015.03.006

984

985 Xiao J (2016) Chemical composition and source identification of rainwater constituents at
986 an urban site in Xi'an. Environ Earth Sci 75:1-12. https://doi.org/10.1007/s12665-015-
987 4997-z

988

989 Yáñez-Serrano A, Bourtsoukidis E, Alves EG, Bauwens M, Stavrakou T, Llusià J, Filella I,
990 Guenther A, Williams J, Artaxo P, Sindelarova K, Doubalova J, Kesselmeier J, Peñuelas J
991 (2020) Amazonian biogenic volatile organic compounds under globalchange. Glob Chang
992 Biol 26:4722-4751. https://doi.org/10.1111/gcb.15185

993

994 Yu Z, Elliott, EM (2017) Novel method for nitrogen isotopic analysis of soil-emitted nitric
995 oxide. Environ. Sci. Technol. 51:6268-6278. https://doi.org/10.1021/acs.est.7b00592

Table 1. Overview of main chemical and isotopic parameters of precipitation samples collected between August 2018 and
November 2019 (N: number of samples, SD: standard deviation).

Variable	$\delta^{18}O$-H_2O (‰)	$\delta^{2}H$-H_2O (‰)	$\delta^{15}N$-NO_3^- (‰)	$\delta^{18}O$-NO_3^- (‰)	pH	NO_3^- (μeq/L)	Cl^- (μeq/L)	SO_4^{2-} (μeq/L)	NH_4^+ (μeq/L)	Na^+ (μeq/L)	Ca^{2+} (μeq/L)	Mg^{2+} (μeq/L)	K^+ (μeq/L)
N	110	110	76	76	109	109	109	109	109	109	109	109	109
Average	-8.61	-59.37	+0.7	+51.7	5.72	22.2	48.5	52.7	31.0	26.0	30.4	13.8	24.6
Median	-8.42	-56.00	+0.7	+52.5	5.55	19.0	28.5	44.1	24.8	27.8	19.5	15.7	17.4
SD	3.45	28.21	2.2	6.5	0.97	13.5	50.6	33.0	27.6	20.7	31.1	8.8	36.7
Minimum	-20.38	-153.35	-3.8	+33.7	4.02	3.0	7.3	14.8	6.7	1.3	3.5	2.5	5.2
Maximum	-0.52	-1.86	+7.1	+65.3	8.18	85.5	372.6	225.3	224.4	120.7	232.4	57.8	299.6

Figures captions

Figure 1. A) Dual isotope diagram for $\delta^{18}O-H_2O$ and δ^2H-H_2O in precipitation (blue circles) used to calculate the local meteoric water line (LMWL, dashed blue line). The global meteoric water line (GMWL) is included as reference. B) and C) Histograms showing δ^2H-H_2O and $\delta^{18}O-H_2O$ values, respectively.

Figure 2: Network correlation diagram based on Pearson´s correlation coefficient for precipitation isotopes, nitrogen isotopes in nitrate, and selected ion composition data (including the precipitation amount, P). Significance (based on p-values) increases as the line thickness increases. Blue and red colors represent positive and negative correlations, respectively. Grouping indicates stronger variable relationships.

Figure 3. Time series plots showing: A) Rainfall (in mm/day, blue bars), B) NO_3^- (in µeq/L, green circles), C) $\delta^{18}O-H_2O$ (in ‰, blue circles), D) $\delta^{15}N-NO_3^-$ (in ‰, red circles), and E) $\delta^{18}O-NO_3^-$ (in ‰, cyan circles). The dry season period when no sampling was carried out is also shown.
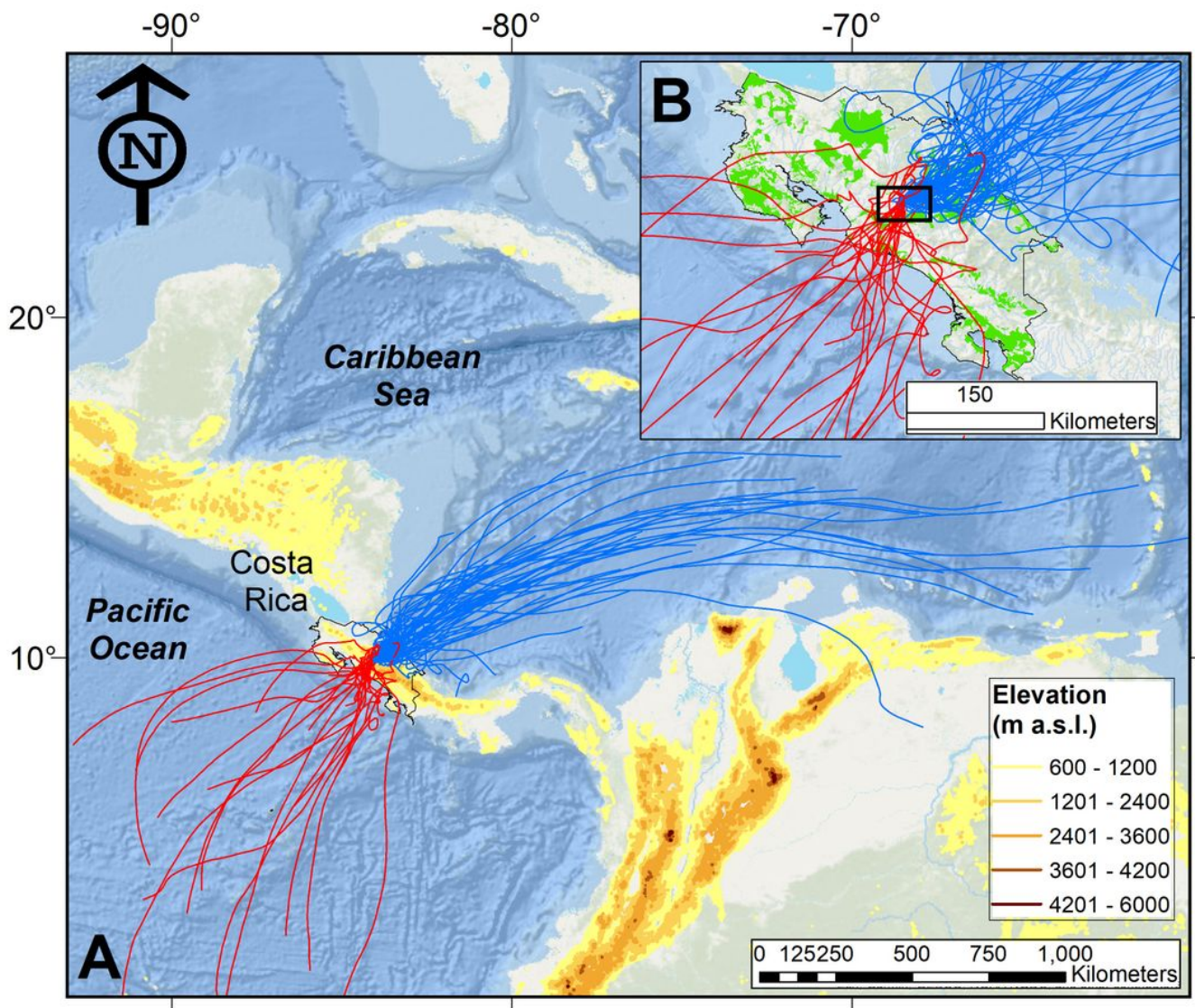
Figure 4. (A) 72-hour air mass back trajectories calculated using the HYSPLIT model for the sampling period August 2018-November 2019 (N=109). Trajectories were separated according to their preferential pathway (i.e., Pacific Ocean: red lines; Caribbean Sea: blue lines). (B) Inset map showing the distribution of the air mass trajectories in relation to the permanent cultivated areas (green-colored areas) located in the Caribbean and Pacific domain of Costa Rica. The black rectangle shows the approximate extension of the Central Valley where most NO_x emissions come from fossil fuels.

Figure 5. Box plots of: A. $\delta^{18}O-H_2O$ (‰), B. NO_3^- (µeq/L), and C. $\delta^{15}N-NO_3^-$ considering air mass trajectory (Caribbean or Pacific). The grey box indicates the 25th and 75th percentiles with the median in middle. The error bars indicate the minimum and maximum values. The black circles indicate outliers (1.5 times the central box).

Figure 6. A) Dual isotope diagram for $\delta^{15}N-NO_3^-$ versus $\delta^{18}O-NO_3^-$ in precipitation. Samples were segregated into Caribbean samples (blue circles, N=59) and Pacific samples (red circles, N=17). Circles were classified into three categories based on the nitrate concentration of this dataset: <16.6 µeq/L (<25th percentile), 16.6-30.8 µeq/L (25th-75th percentile), and > 30.8 µeq/L (>75th percentile). The average ± standard deviation values of $\delta^{15}N-NO_3^-$ and $\delta^{18}O-NO_3^-$ are shown as reference. B) and C) Histograms showing the $\delta^{15}N-NO_3^-$ and $\delta^{18}O-NO_3^-$ values, respectively.

Figure 7. Bar plot showing the Bayesian model results of proportion and error estimations of NO_x emission sources contributing to the wet deposition in the Central Valley of Costa Rica. Precipitation samples were classified according to the preferential air mass pathway (Caribbean Sea: black bars, Pacific Ocean: gray bars). The average ε value of 8.89‰ calculated with reference to percent formation pathways is applied to correct for N fractionation.
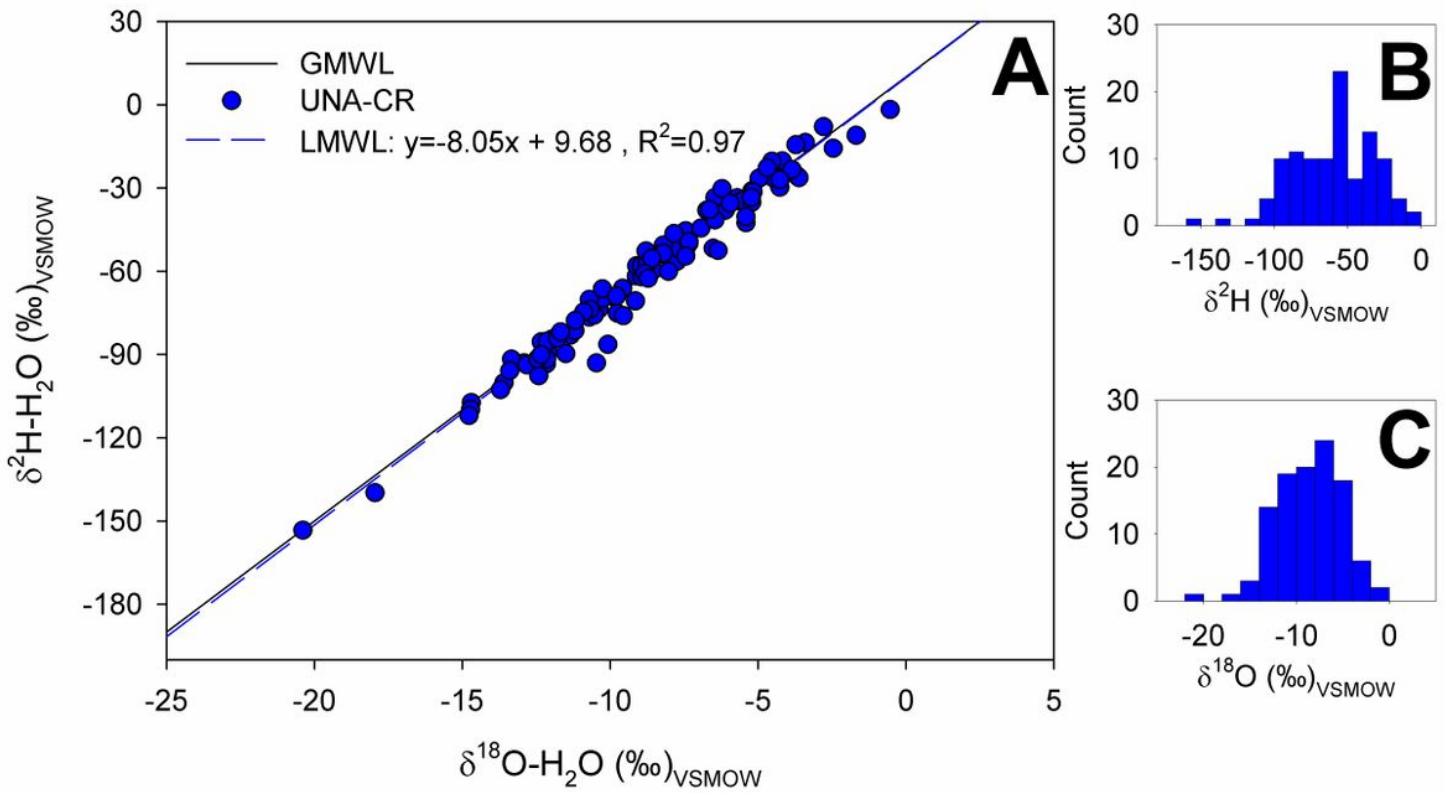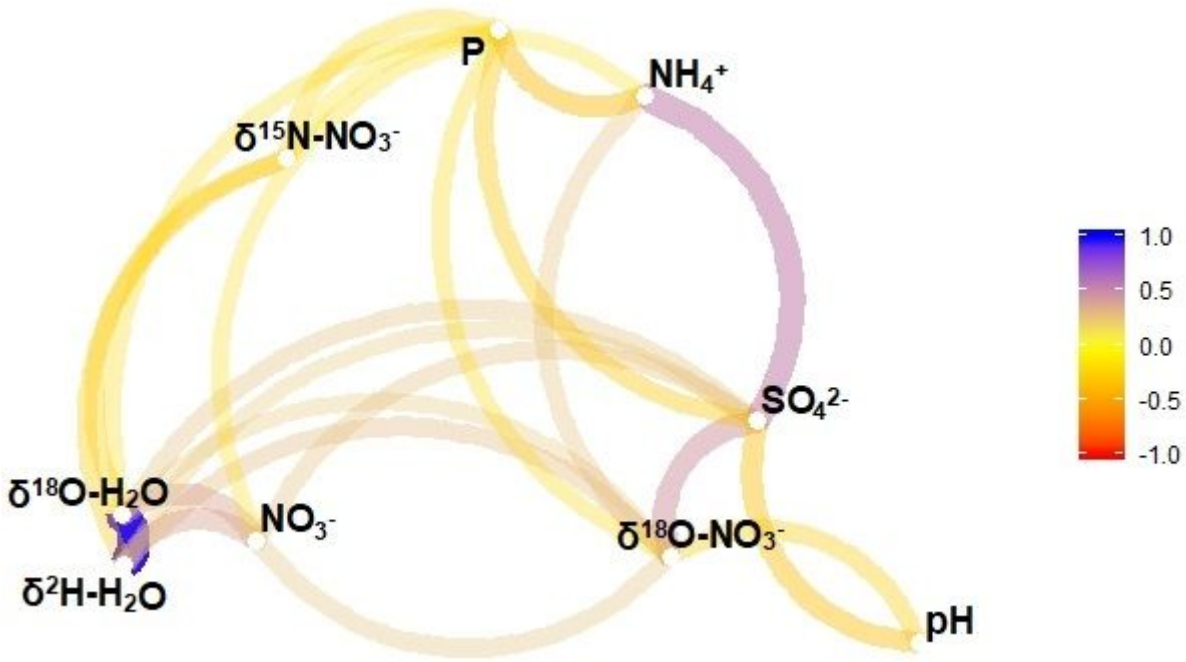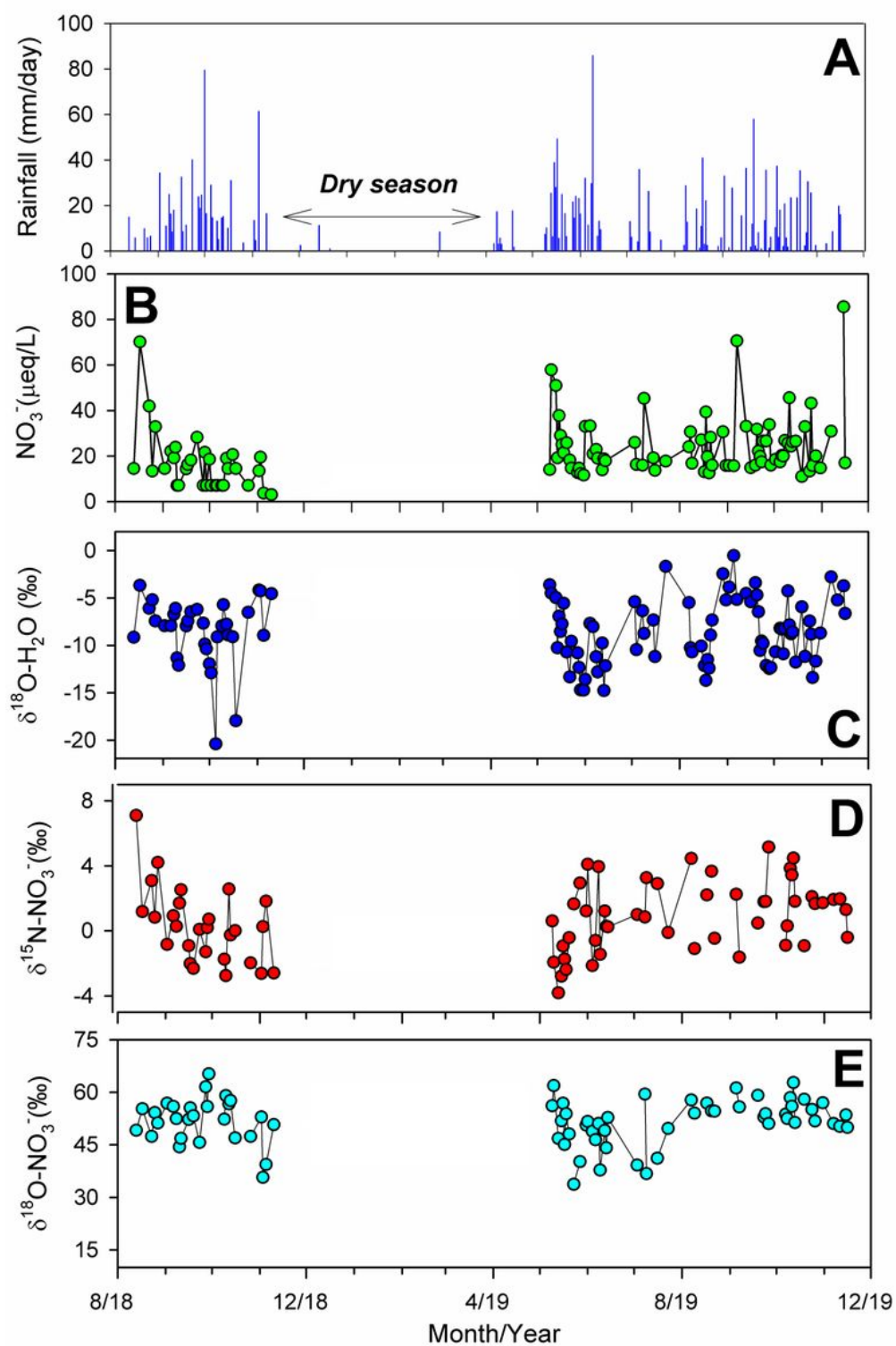
Figures

Figure 1

A) Dual isotope diagram for δ18O-H2O and δ2H-H2O in precipitation (blue circles) used to calculate the local meteoric water line (LMWL, dashed blue line). The global meteoric water line (GMWL) is included as reference. B) and C) Histograms showing δ2H-H2O and δ18O-H2O values, respectively.

Figure 2

Network correlation diagram based on Pearson's correlation coefficient for precipitation isotopes, nitrogen isotopes in nitrate, and selected ion composition data (including the precipitation amount, P). Significance (based on p-values) increases as the line thickness increases. Blue and red colors represent positive and negative correlations, respectively. Grouping indicates stronger variable relationships.

Figure 3

Time series plots showing: A) Rainfall (in mm/day, blue bars), B) NO3- (in µeq/L, green circles), C) δ18O-H2O (in ‰, blue circles), D) δ15N-NO3- (in ‰, red circles), and E) δ18O-NO3- (in ‰, cyan circles). The dry season period when no sampling was carried out is also shown.

Figure 4

(A) 72-hour air mass back trajectories calculated using the HYSPLIT model for the sampling period August 2018-November 2019 (N=109). Trajectories were separated according to their preferential pathway (i.e., Pacific Ocean: red lines; Caribbean Sea: blue lines). (B) Inset map showing the distribution of the air mass trajectories in relation to the permanent cultivated areas (green-colored areas) located in the Caribbean and Pacific domain of Costa Rica. The black rectangle shows the approximate extension of the Central Valley where most NOx emissions come from fossil fuels.

Figure 5

Box plots of: A. δ18O-H2O (‰), B. NO3- (µeq/L), and C. δ15N-NO3- considering air mass trajectory (Caribbean or Pacific). The grey box indicates the 25th and 75th percentiles with the median in middle. The error bars indicate the minimum and maximum values. The black circles indicate outliers (1.5 times the central box).
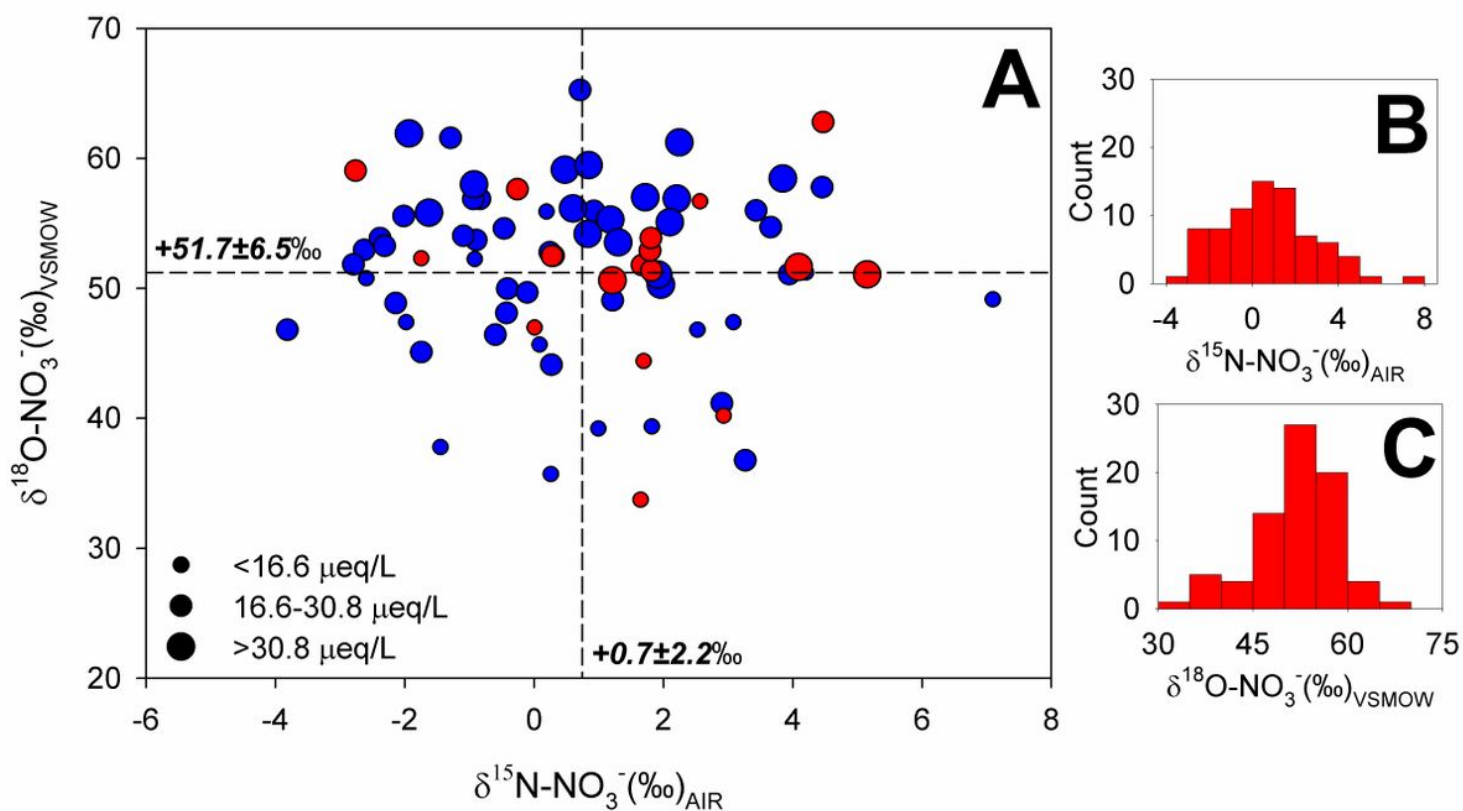
Figure 6

A) Dual isotope diagram for δ15N-NO3- versus δ18O-NO3- in precipitation. Samples were segregated into Caribbean samples (blue circles, N=59) and Pacific samples (red circles, N=17). Circles were classified into three categories based on the nitrate concentration of this dataset: <16.6 μeq/L (<25th percentile), 16.6-30.8 μeq/L (25th-75th percentile), and > 30.8 μeq/L (>75th percentile). The average ± standard deviation values of δ15N-NO3- and δ18O-NO3- are shown as reference. B) and C) Histograms showing the δ15N-NO3- and δ18O-NO3- values, respectively.
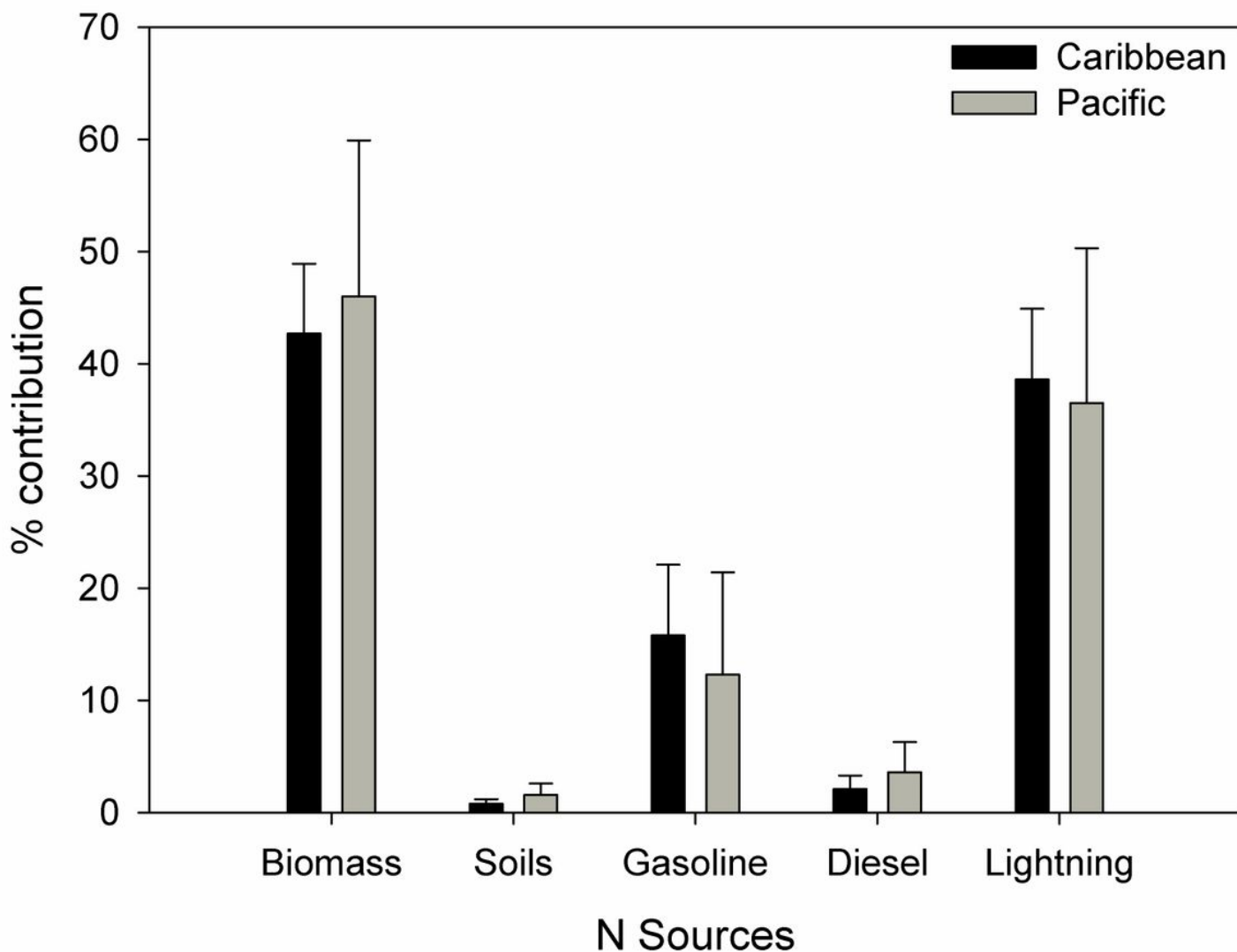
Figure 7

Bar plot showing the Bayesian model results of proportion and error estimations of NOx emission sources contributing to the wet deposition in the Central Valley of Costa Rica. Precipitation samples were classified according to the preferential air mass pathway (Caribbean Sea: black bars, Pacific Ocean: gray bars). The average ε value of 8.89‰ calculated with reference to percent formation pathways is applied to correct for N fractionation.